catalysts

MDPI

Review

Antiviral Effect of Visible Light-Sensitive Cu_xO/TiO_2 Photocatalyst

Masahiro Miyauchi [1,*], Kayano Sunada [2] and Kazuhito Hashimoto [3,*]

1 Department of Materials Science and Engineering, School of Materials and Chemical Technology, Tokyo Institute of Technology, 2-12-1, Ookayama, Meguro-ku, Tokyo 152-8552, Japan
2 Kanagawa Institute of Industrial Science and Technology (KISTEC), 3-25-13, Tonomachi, Kawasaki, Kanagawa 210-0821, Japan; pg-sunada@newkast.or.jp
3 National Institute for Materials Science (NIMS), 1-2-1 Sengen, Tsukuba, Ibaraki 305-0047, Japan
* Correspondence: mmiyauchi@ceram.titech.ac.jp (M.M.); HASHIMOTO.Kazuhito@nims.go.jp (K.H.); Tel.: +81-3-5734-2527 (M.M.); +81-29-859-2856 (K.H.)

Received: 1 September 2020; Accepted: 18 September 2020; Published: 21 September 2020

Abstract: Photocatalysis is an effective technology for preventing the spread of pandemic-scale viruses. This review paper presents an overview of the recent progress in the development of an efficient visible light-sensitive photocatalyst, i.e., a copper oxide nanoclusters grafted titanium dioxide (Cu_xO/TiO_2). The antiviral Cu_xO/TiO_2 photocatalyst is functionalised by a different mechanism in addition to the photocatalytic oxidation process. The Cu_xO nanocluster consists of the valence states of Cu(I) and Cu(II); herein, the Cu(I) species denaturalizes the protein of the virus, thereby resulting in significant antiviral properties even under dark conditions. Moreover, the Cu(II) species in the Cu_xO nanocluster serves as an electron acceptor through photo-induced interfacial charge transfer, which leads to the formation of an anti-virus Cu(I) species and holes with strong oxidation power in the valence band of TiO_2 under visible-light irradiation. The antiviral function of the Cu_xO/TiO_2 photocatalyst is maintained under indoor conditions, where light illumination is enabled during the day but not during the night; this is because the remaining active Cu(I) species works under dark conditions. The Cu_xO/TiO_2 photocatalyst can thus be used to reduce the risk of virus infection by acting as an antiviral coating material.

Keywords: photocatalysis; antiviral; visible light; copper oxide; titanium dioxide; interfacial charge transfer; SARS-CoV-2

1. Introduction

Human beings have suffered from numerous kinds of pandemic viruses, such as SARS [1], Ebola virus [2], H1N2/2009 influenza [3], and COVID-19 (SARS-CoV-2) [4]. These viruses spread through direct person-to-person contact and/or indirect contact via virus-containing airborne droplets or contaminated surfaces of objects such as floors, handrails, touch panel/buttons, or furniture [5]. Therefore, antiviral chemicals and/or materials are useful for protecting against the spread of pandemic-scale viruses. For example, alcohol [6], hydrogen peroxide [7], and hypochlorous acid [8] have been widely used to disinfect various objects against bacteria or viruses. These chemicals deactivate viruses by denaturising their proteins [9]. However, the antiviral effect of these chemicals is not sustainable over the long term because of their evaporation and/or dissipation. Conversely, solid-state antiviral metal compounds could be useful because of their robustness and feasibility for use as coating materials. Although the biocidal properties of copper and silver have been reported previously [10], their antiviral effects are insufficient and do not last over the long term. Once their

surfaces become contaminated by organic molecules, contact between the active metal and the viruses is inhibited.

Among various antiviral materials, the titanium dioxide (TiO_2)-based photocatalysts are promising [11–14], because their antiviral effect is functioned under ultraviolet (UV) light irradiation [15,16]. Photogenerated holes in the valence band of TiO_2 exhibit strong oxidation power for decomposing organic molecules [17–19]; thus, virus components such as surface proteins are oxidized under UV irradiation, resulting in virus disinfection [12]. Furthermore, a TiO_2 photocatalyst film has a self-cleaning function by the strong oxidation power of holes [20] and its super-hydrophilic function [21–25], which helps the film retain its clean surface under UV light. Thus, surface contaminants are removed to expose antiviral active sites. However, TiO_2 can only be activated by UV light, which is hardly contained in normal room light. Because viral infections mainly occur in indoor environments, it is necessary to use a visible light-sensitive antiviral photocatalyst. It is also noted that lighting is usually turned off during the night; thus, the sustained antiviral properties of photocatalysts under dark conditions are also important for their practical use.

Recently, we developed an efficient visible light-sensitive photocatalyst based on Cu(II) oxide nanoclusters grafted onto TiO_2 [Cu(II)/TiO_2] by using the concept of interfacial charge transfer (IFCT) [26–32]. Although the Cu(II)/TiO_2 photocatalyst exhibited efficient photocatalytic oxidation activity and antiviral properties under visible light irradiation, its antiviral activity under dark conditions was limited. To improve the antiviral activity in the dark, we further developed Cu_xO ($1 < x < 2$) nanoclusters, which consisted of Cu(I) and Cu(II) species, and grafted them onto the TiO_2 surface (denoted as Cu_xO/TiO_2) [33]. While the Cu(II) species in Cu_xO nanoclusters is indispensable for the photocatalysis process, the Cu(I) species plays a crucial role in denaturing virus proteins, thereby causing their disinfection under dark conditions [33–35].

This review paper explains the role of the Cu(I) and Cu(II) species on TiO_2 in terms of efficient antiviral activity. We first introduce the antiviral properties of pristine copper oxides (CuO and Cu_2O) under dark conditions in the next section on the basis of our previous reports [34,35] and discuss the role of the Cu(I) species in Cu_2O in terms of its antiviral properties. We then show the disadvantage of Cu_2O for practical use because its surface can easily be oxidized into the inactive Cu(II) state in ambient humid air. Subsequently, we introduce our recent studies regarding Cu(II)/TiO_2 as a visible light-sensitive photocatalyst [26,27,32], and Cu_xO/TiO_2 as a visible light-sensitive as well as an efficient antiviral catalyst even under dark conditions [33]. The characterization, photocatalytic working principle, and sustained antiviral mechanism of these materials have been presented in this paper. We also show the results of the antiviral tests using a pseudo splash-containing bacteriophage Qβ on Cu_xO/TiO_2-coated sheet fabric. This review paper comprehensively introduces the practical advantage of using Cu_xO/TiO_2 as an antiviral coating material to protect against the spread of pandemic-scale viruses.

2. Antiviral Effect of Pristine Copper Oxides (CuO and Cu_2O) Under Dark Conditions

While copper-based compounds are used as a catalyst [36,37], copper oxides have been previously reported to have antimicrobial activity [38–40]. In our previous studies, the antiviral effects of CuO and Cu_2O coated on glass substrates were reported [34,35]. Figure 1 shows the antiviral properties of CuO and Cu_2O films under dark conditions. In this experiment, two types of viruses with different surface structures, the H1N1 influenza A virus (A/PR8/H1N1) and bacteriophage Qβ were examined. The influenza A virus possesses a viral envelope, a cell membrane-like structure that encases its central core, whereas bacteriophages lack an envelope; instead, their surface is composed of protein capsids. As shown in Figure 1, the titers of influenza A and bacteriophage Qβ drastically decreased upon contact with Cu_2O by several orders of magnitude even after 30 min, whereas the CuO was not active against either influenza A or bacteriophage Qβ. We also compared the antiviral properties of CuS and Cu_2S and found that those of Cu_2S were significantly superior to those of CuS [34]. These results strongly indicate that the Cu(I) species plays an important role for efficient antiviral properties.

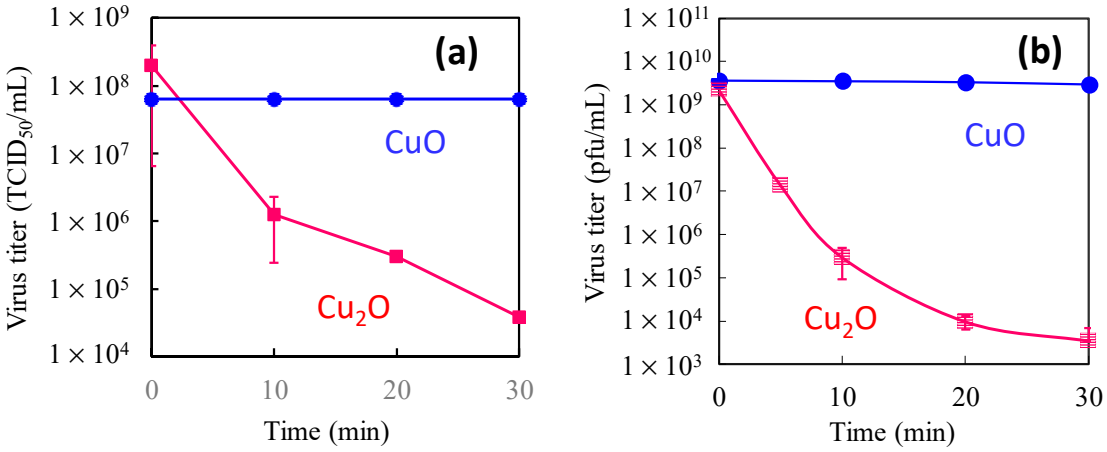

Figure 1. (**a**) Titer of influenza A virus and (**b**) bacteriophage Qβ as a function of exposure time to Cu_2O (red squares) and CuO films (blue circles) [35]. Error bars indicate standard deviations of two or three replicate experiments. CuO and Cu_2O powder were coated on glass substrates and their antiviral test was examined under room temperature. These experimental methods are based on the protocols (ISO 18184:2014 Textiles—Determination of antiviral activity of textile products, and ISO 18071:2016 Fine ceramics—Determination of antiviral activity of semiconducting photocatalytic materials under indoor lighting environment—Test method using bacteriophage Q-beta).

We anticipated three plausible reasons for the efficient antiviral properties of Cu_2O, as shown in Figure 2: (a) reactive oxygen species (ROS) [41], (b) leached copper ions [10], and (c) the solid-state compound itself [34,35]. Based on our careful investigation, we excluded ROS by evaluating the antiviral properties under nitrogen atmosphere. The antiviral activity of Cu_2O under nitrogen was consistent with that under oxygen atmosphere, indicating that ROS did not contribute to the antiviral activity of Cu_2O. It was also found that leached copper ions did not influence the antiviral activity of Cu_2O according to a control experiment using a copper ion solution [34]. Therefore, the most plausible reason for the efficient antiviral properties of Cu_2O is the solid-state Cu_2O compound itself involving Cu(I) species. There are several experimental results that support the importance of direct physical contact between Cu_2O and viruses [34]. For example, we inserted a 105 μm thickness of filter paper (pore size = 30 nm) between the Cu_2O-coated glass substrate and the viral suspension, which inhibited the antiviral properties of the Cu_2O [34]. Furthermore, we chemically modified the Cu_2O surface with 1H-benzotriazole (BTA), which strongly coordinates with surface copper atoms via the nitrogen atoms of its triazole ring [42], and the results showed that the antiviral properties of Cu_2O treated with BTA were significantly worse than those of untreated Cu_2O [34]. These results strongly imply that the surface of Cu_2O causes the denaturation or degradation of biomolecules in viruses, which results in their inactivation.

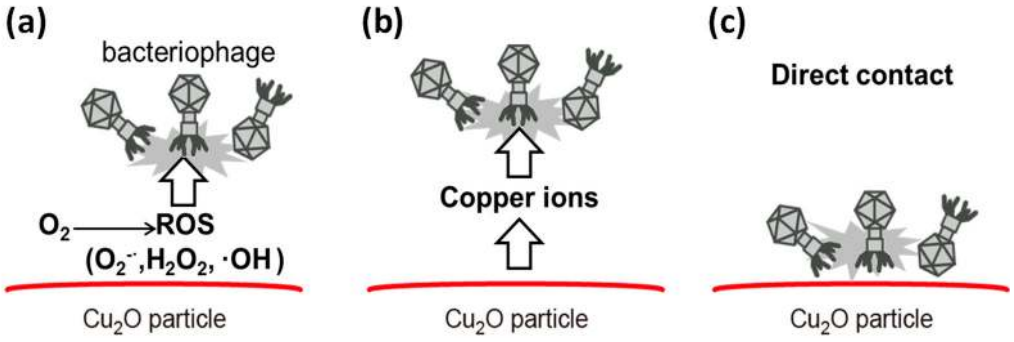

Figure 2. Possible mechanisms of the antiviral activity of Cu_2O: (**a**) reactive oxygen species (ROS), (**b**) leached copper ions, and (**c**) direct contact with the surface [34].

To verify the distinctive antiviral mechanism of Cu_2O, we investigated the adsorption properties of model protein molecules [bovine serum albumin (BSA)] on the surface of Cu_2O, because the outer capsids of bacteriophage Qβ are composed of protein molecules. Figure 3a shows the adsorption properties of Cu_2O in comparison with those of CuO and silver (Ag) as control groups. We used Ag for comparison because metallic Ag compounds have also been reported as effective anti-bacterial materials [43–46]. As shown in Figure 3a, the incubation of a 130 ng/mL solution of BSA with Cu_2O for 8 h resulted in a 30% decrease in the supernatant concentration, revealing strong protein adsorption onto the solid-state Cu_2O. Conversely, BSA adsorption onto CuO and Ag was limited. Furthermore, we investigated the protein denaturation by measuring the enzyme activity of alkaline phosphatase as a model enzyme, and the results are shown in Figure 3b. After exposure of the enzyme to Cu_2O for 1 h, the enzyme activity decreased to 30% and 50% of the original activity at enzyme concentrations of 148 and 240 ng/mL, respectively. However, after exposure to CuO or Ag, the active enzyme concentration did not decrease from that of its original state. These results strongly imply that the protein adsorption and denaturation abilities of solid-state Cu_2O are significantly higher than those of CuO and Ag, resulting in strong deactivation of bacteriophage Qβ.

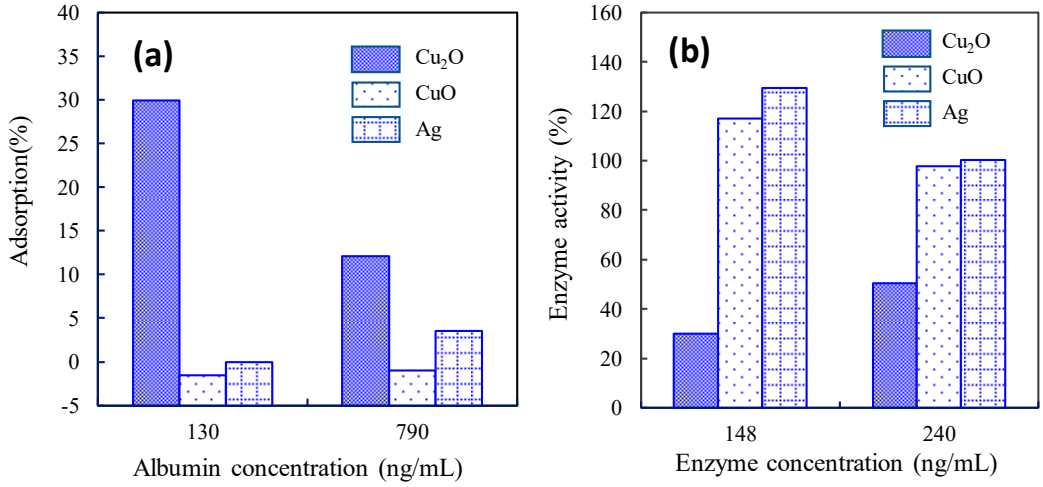

Figure 3. (**a**) Adsorption properties of bovine serum albumin (BSA) onto Cu_2O, CuO, and Ag after 8 h exposure. Panel (**b**) shows enzyme activities of these materials after 1 h exposure [34]. These data are based on average of triplicate measurements.

To further verify the disinfection of influenza viruses by Cu_2O, we focused on the viral surface proteins that are highly involved in the infection process. Influenza viruses consist of hundreds of haemagglutinin (HA) and neuraminidase (NA) protein groups on the envelope surface. HA is a glycosylated lectin protein that recognizes sialic acid residues on the receptor proteins of the host cells [47]. Once influenza viruses bind through the HA-sialic acid interaction, they can enter the host cells through endocytosis. NA is an endoglycosidase that is necessary for the release of viruses from the surfaces of host cells; it is also involved in the initiation of influenza infection [48]. Both proteins play important roles in the spread of influenza infection. To determine HA activity after exposure to copper oxides, the HA protein was incubated and mixed with chicken red blood cells [49]. To determine NA activity, the 1,2-dioxetane derivative of sialic acid (NA-STAR) was used as a chemiluminescence substrate for highly sensitive detection [50]. Figure 4a,b show the changes in HA and NA activity. After exposure to Cu_2O, the HA titer drastically decreased and fell below the detection limit within 30 min. Conversely, the HA titer after exposure to CuO did not change over 30 min. Similarly, NA activity decreased after exposure to Cu_2O after 10 min, whereas NA activity was not influenced by exposure to CuO. These results reveal that both the haemagglutination ability of HA and the enzymatic activity of NA are disrupted by exposure to Cu_2O. Based on these results, we can conclude that the protein denaturation property of Cu_2O yields efficient antiviral function, even under dark conditions.

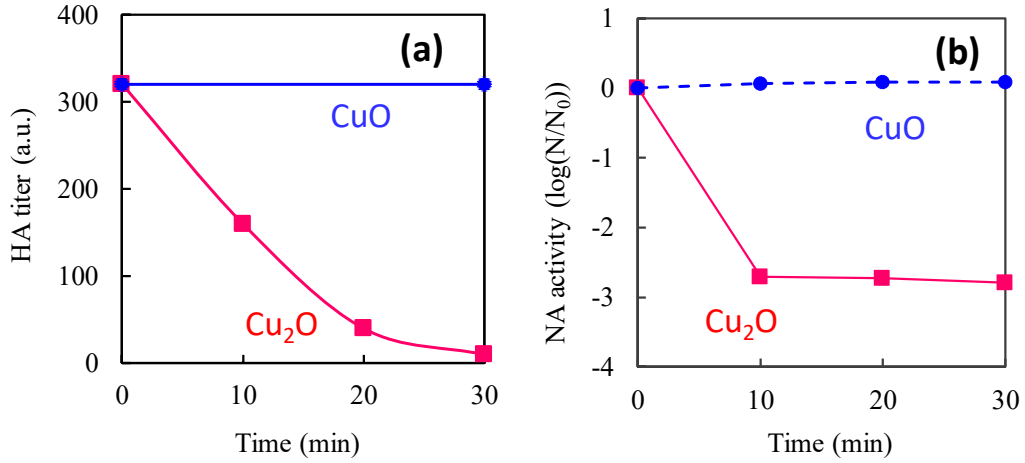

Figure 4. Hemagglutinin (HA) titer and neuraminidase (NA) activity exposed to Cu_2O and CuO suspensions. Effect on (**a**) HA titer and (**b**) NA activity of Cu_2O (red squares) and CuO (blue circles) as determined by a hemagglutination test and chemiluminescence using the NA-Star method, respectively. N_0 in panel (**b**) is the initial NA amount [35]. These data are based on an average of triplicate measurements.

Although Cu_2O exhibits strong antiviral properties, Cu(I) is easily oxidized to Cu(II) states under ambient humid atmosphere. In fact, the antiviral properties of Cu_2O exposed to humid air (relative humidity 90% at 25 °C) for one week or two weeks significantly worsened compared to those of fresh Cu_2O (Figure 5). These results indicate that the antiviral activity of Cu_2O is decreased by its self-oxidation [51]. Platzman et al. reported that the Cu_2O surface transformed to a copper hydroxide [$Cu(OH)_2$] metastable state with several nanometres in thickness, due to the interactions of Cu ions with hydroxyl groups present at the surface [52]. Further, the metastable $Cu(OH)_2$ phase transformed into a stable CuO layer [51,52]. Therefore, keeping Cu(I) species on the surface of Cu_2O under ambient conditions is important for achieving the sustained antiviral activity of Cu_2O.

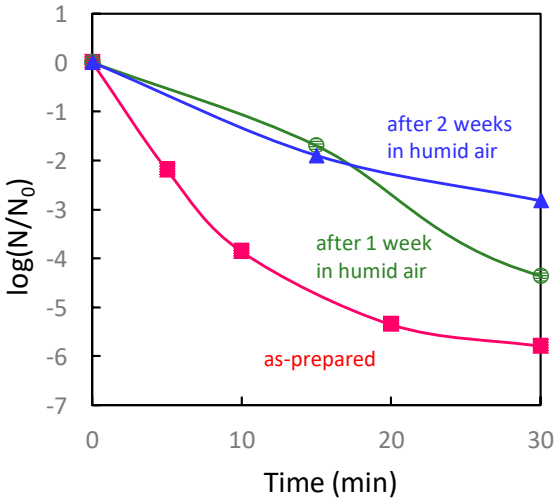

Figure 5. Antiviral properties of Cu_2O after a week storage in 90% humid air atmosphere (green circles), those after two weeks storage in 90% humid air (blue triangles), and those of as-prepared sample using fresh Cu_2O powder (FUJIFILM Wako Pure Chemical Corporation) taken from a commercial bottle (red squares). The data were based on averages of triplicate measurements for as-prepared sample, while duplicate measurements for 1 and 2 weeks after samples.

3. Visible Light-Sensitive Cu(II)/TiO_2 Photocatalyst

The previous section suggests that maintaining the Cu(I) species is critical for sustaining antiviral properties over the long term. The main goal of this paper is to introduce the combination of a TiO_2 photocatalyst with Cu_xO nanoclusters containing Cu(I) and Cu(II) species to achieve sustained antiviral properties. Before providing a detailed explanation of the Cu_xO/TiO_2 system, we describe the role of the Cu(II) species attached to the TiO_2 photocatalyst.

We previously reported Cu(II) nanoclusters grafted onto TiO_2 [Cu(II)/TiO_2] as an efficient visible light-sensitive photocatalyst for the oxidation of organic molecules [26,27]. Cu(II) nanoclusters could be grafted onto TiO_2 (rutile, MT-150A, TAYCA Corporation) by wet chemical impregnation method using copper chloride dissolved aqueous media (0.1 wt % versus TiO_2) as reported in our previous studies [26,27]. Figure 6a shows a transmission electron microscope (TEM) image of Cu(II)/TiO_2, where Cu(II) clusters a few nanometres in size were grafted onto the TiO_2 surface. Although the size of the Cu(II) nanocluster was too small to detect its X-ray diffraction, a previous study determined the local chemical structure of the Cu(II) nanoclusters by X-ray absorption near-edge structure (XANES) and extended X-ray absorption fine structure (EXAFS) [27]. Figure 6b shows the XANES spectra of Cu(II)/TiO_2 and commercial reference powders. The spectrum of Cu(II)/TiO_2 resembles that of $Cu(OH)_2$, indicating that the valence number of the nanoclusters is in the 2+ state and that the Cu(II) species are likely to be in the five-coordinate square pyramidal form [53–55]. Figure 6c shows the EXAFS results of Cu(II)/TiO_2 and commercial powder references of $Cu(OH)_2$ and CuO. In contrast to the XANES results, the local chemical environment of the Cu(II) nanoclusters resembles that of CuO. The EXAFS data were carefully analysed using the REX2000 (Rigaku Corporation) and the FEFF program [56], and a one-coordinate Cu–O bond length (2.1–2.2 Å) was observed in $Cu(OH)_2$ and Cu(II)/TiO_2. Thus, the grafted Cu(II) nanoclusters are in the five-coordinate environment, which is consistent with the XANES results. In addition, one four-coordinate Cu–Cu and three types of two-coordinate Cu–Cu were observed, and the Cu–Cu bond lengths were similar to those in CuO, and so it can be considered that the grafted Cu(II) nanoclusters resemble the chemical environment of Cu(II) in CuO. That is, the local structure of the Cu(II) nanoclusters is distorted CuO, wherein the apical oxygen approaches Cu(II), forming a five-coordinate square pyramid attached to the TiO_2 surface [27].

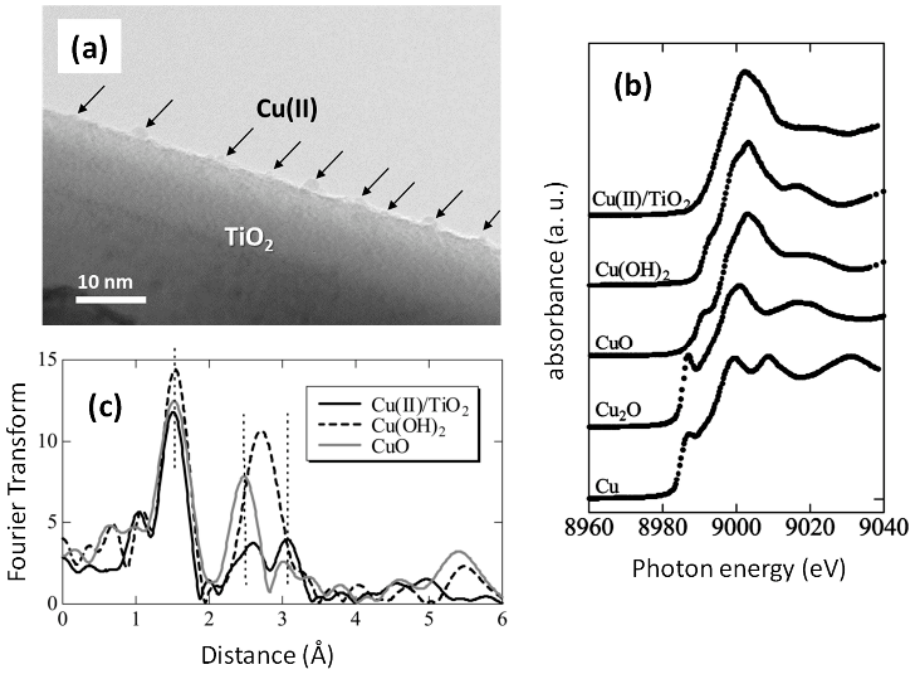

Figure 6. (**a**) TEM image, (**b**) XANES analyses, and (**c**) Fourier transforms of EXAFS for Cu(II)/TiO_2 [27]. Commercial powder of Cu, Cu_2O, CuO, and $Cu(OH)_2$ (Wako Ltd.) were used as references.

Figure 7a shows the UV-vis absorption spectra of pristine TiO_2 and Cu(II)/TiO_2. The pristine TiO_2 exhibited strong UV light absorption shorter than 400 nm owing to its bandgap excitation. Meanwhile, Cu(II)/TiO_2 exhibited additional visible-light absorption around 400–480 nm and over 650 nm. The former absorption is owing to the inter facial charge transfer (IFCT) excitation from the valence band of TiO_2 to the Cu(II) nanocluster [26,27], whereas the latter originates in the d–d transition in the Cu(II) species [57]. The IFCT process is theoretically feasible between a semiconductor and ligand under photon irradiation [58], and visible-light absorption through IFCT was experimentally observed in previous studies [59–61]. The IFCT transition was also observed in the iron oxide-based Fe(III) nanocluster-grafted TiO_2 [31,62].

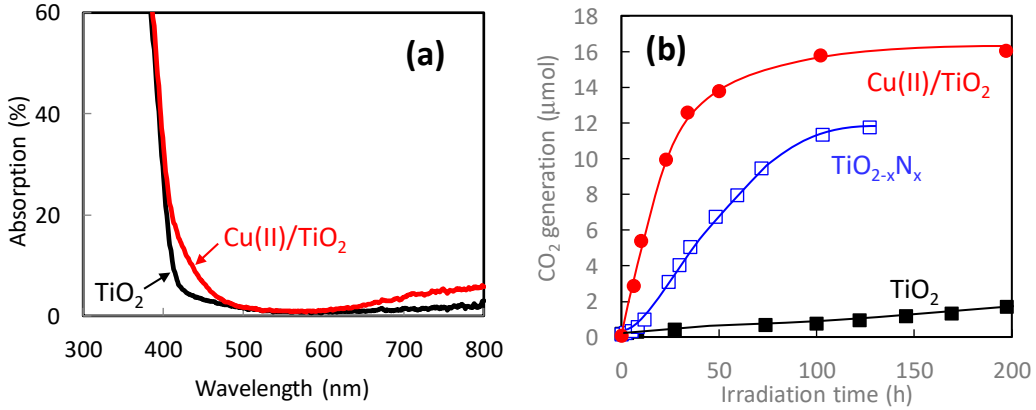

Figure 7. (**a**) Optical absorption spectra of TiO_2 (black line) and Cu(II)/TiO_2 (red line). Amount of Cu(II) was 0.1 wt% versus TiO_2 particles. (**b**) Photocatalytic oxidation activities of 2-propanol under visible-light irradiation for bare TiO_2 (black), $TiO_{2-x}N_x$ (blue), and Cu(II)/TiO_2 (red). Visible-light irradiation was conducted using a xenon lamp passed through optical filters to set the wavelength at 400–530 nm with an illuminance of 1 mW/cm^2.

Figure 7b shows the photocatalytic oxidation activities of gaseous 2-propanol to carbon dioxide (CO_2) under visible-light irradiation. As control groups, we also evaluated the photocatalytic activities of bare TiO_2 and nitrogen-doped TiO_2 ($TiO_{2-x}N_x$). The $TiO_{2-x}N_x$ photocatalyst, which is recognized as an efficient visible-light photocatalyst [63], was prepared by a wet chemical method using titanium tetrachloride and ammonia, similar to a previous report [64]. The activity of pristine TiO_2 was limited because of the lack of its visible-light absorption. In the case of $TiO_{2-x}N_x$, CO_2 molecules were generated by the oxidation of 2-propanol; however, its activity was worse than that of Cu(II)/TiO_2 because of the lower oxidation power of the holes excited in the nitrogen orbital [65–67]. It is noted that the Cu(II)/TiO_2 photocatalyst decomposed 2-propanol with an initial amount of 5 μmol, producing approximately 15 μmol of CO_2, showing that complete decomposition was achieved under visible-light irradiation. The quantum efficiency of the Cu(II)/TiO_2 system reached over 80% by the optimization of the fabrication process [29], and thus it was significantly superior to that of $TiO_{2-x}N_x$ [65,66].

The mechanism of the photocatalytic reaction by Cu(II)/TiO_2 was previously investigated by various spectroscopic analyses. For example, Nosaka et al. examined the in situ electron spin resonance (ESR) of Cu(II)/TiO_2 under visible-light irradiation [68]. Cu(II) species involve unpaired electrons, thus exhibiting an ESR signal, whereas Cu(I) is ESR-inactive. Furthermore, the photogenerated electrons and holes in TiO_2 can be detected by ESR. When the Cu(II)/TiO_2 sample was irradiated by visible light under vacuum conditions, the ESR signal of the Cu(II) species decreased and that of photogenerated holes in the valence band of TiO_2 appeared. These results strongly suggest that the electron transition occurs from the valence band of TiO_2 to the Cu(II) species through their interface under visible-light irradiation to generate Cu(I) species and holes in TiO_2. The signal of the photogenerated holes decreased by the introduction of gaseous 2-propanol into the ESR chamber, whereas that of Cu(II) recovered by exposure to oxygen [68]. These results also indicate that the photogenerated holes

oxidize 2-propanol, whereas excited electrons in the copper ion species react with oxygen molecules. Formation of Cu(I) species on TiO_2 under light irradiation was also reported in the other previous literature [69]. The redox potential of Cu(II)/Cu(I) is approximately 0.16 V [versus a normal hydrogen electrode (NHE)] [26,27], which is more negative than that of the multi-electron reduction reaction of oxygen molecules to hydrogen peroxide (0.68 V vs. NHE) [70–72]. Therefore, excited electrons in the Cu(I) species react with oxygen molecules through a multi-electron reduction process under an oxygen-abundant atmosphere. A similar electron transition trend was seen in the XANES results [27]. Furthermore, Osako et al. visualized the reduction and oxidation sites in a Cu(II)/TiO_2 system by using an ultrathin CuO film with a well-defined pattern coated onto a TiO_2 single crystal prepared by pulsed laser deposition and photolithography [73]. Using an atomic force microscope (AFM), the authors observed the formation of metal Ag particles on the film resulting from the photoreduction of Ag^+ ions, and Ag particles were selectively deposited on the edge of a CuO film under visible-light irradiation [74]. These results also suggest that the IFCT transition occurs by visible light and that the Cu(II) species acts as reduction sites. The concept of an IFCT transition for the development of visible light-sensitive photocatalysts has been extended to semiconductor systems other than TiO_2, such as ZnO [75,76], $SrTiO_3$ [77,78], SnO_2 [79], $Nb_3O_8^-$ [80], Ag_3PO_4, Bi_2O_3 [81], BiOCl [82], $BiVO_4$ [83], and Ag-based compounds [84]. The concept of an IFCT transition was also adopted for impurity-doped TiO_2, such as Ti(III) self-doped TiO_2 [28], Nb(IV)-doped TiO_2 [85], and W(IV) and Ga(III)-codoped TiO_2 [86].

Figure 8 shows the antiviral bacteriophage Qβ activity of $TiO_{2-x}N_x$ and Cu(II)/TiO_2 under white-light irradiation and dark conditions. Among these samples, the antiviral activity of Cu(II)/TiO_2 under white-light irradiation was the most significant. Even though $TiO_{2-x}N_x$ exhibited photocatalytic oxidation activity for 2-propanol [Figure 7b], its antiviral activity was negligible, attributed to its limited oxidation power [65–67]. In contrast, the number of bacteriophage Qβ on contact with Cu(II)/TiO_2 under white-light irradiation decreased more than two orders of magnitude after 60 min of exposure. The antiviral properties of Cu(II)/TiO_2 under dark conditions, however, were limited because the Cu(II) species was not as effective for the disinfection of viruses, as described in the previous section.

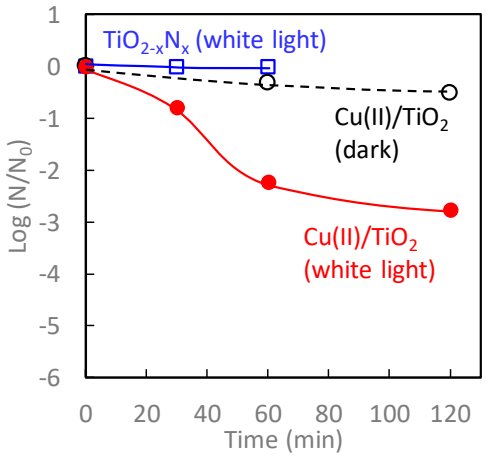

Figure 8. Antiviral bacteriophage Qβ for Cu(II)/TiO_2 under dark (black), $TiO_{2-x}N_x$ under white-light irradiation (blue), and Cu(II)/TiO_2 under white-light irradiation (red). Light irradiation was conducted using a commercial 10 W cylindrical white fluorescent lightbulb (FL-10, Mitsubishi) with a UV cut-off film shorter than 400 nm at an illuminance of 800 lux, which was measured by photometer (Topcon IM-5).

Through the IFCT transition in Cu(II)/TiO_2, the Cu(I) species are created, in addition to the generation of holes in the valence band of TiO_2. The produced Cu(I) species are effective for protein denaturation, and the holes, which have strong oxidation power, causing protein decomposition, and leading to virus disinfection. The contribution of the Cu(I) species generated by an IFCT transition to the antiviral properties was suggested by a previously reported "pre-irradiation" experiment [32].

Figure 9 shows the antiviral activities of Cu(II)/TiO_2 under dark conditions without/with pre-irradiation. As a pre-irradiation treatment, the Cu(II)/TiO_2 sample was placed under a white fluorescence lightbulb passed through a UV cut-off film below 400 nm before the evaluation of the antiviral effect. After the pre-irradiation treatment, the Cu(II)/TiO_2 film was subjected to antiviral activity testing using bacteriophage Qβ under dark conditions. As shown in Figure 9, the pre-irradiation treatment improved the antiviral activity of Cu(II)/TiO_2. This result suggests that pre-irradiation produced the Cu(I) species through the IFCT process, and some of them reacted with oxygen molecules in air, but the others remained even in the dark for a while, causing an antiviral effect. The previous study also showed that pre-irradiation with UV light improved the antiviral activity of Cu(II)/TiO_2 [32], indicating that the excited electrons in the conduction band of TiO_2 would also be injected into Cu(II) nanoclusters to form Cu(I) species.

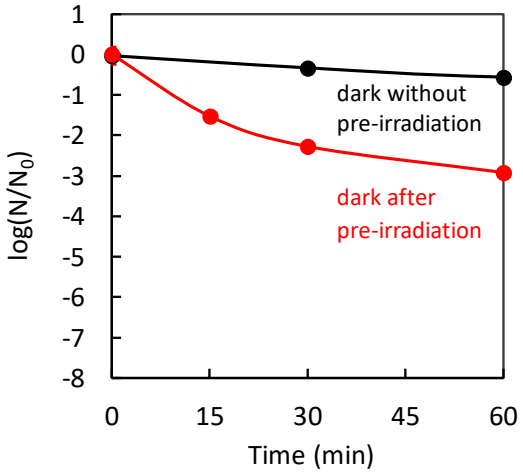

Figure 9. Inactivation of bacteriophage Qβ by Cu(II)/TiO_2 under dark conditions without pre-irradiation (black) and after pre-irradiation treatment (red) [32]. The pre-irradiation treatment was conducted using a white fluorescence lightbulb passed through a UV cut-off film below 400 nm.

4. Antiviral Cu_xO/TiO_2 Photocatalyst

Although Cu(II)/TiO_2 exhibited efficient antiviral properties under visible-light irradiation, its antiviral function under dark conditions was limited as shown in Figure 8. Here, we introduce the Cu_xO ($1 < x < 2$) nanoclusters grafted TiO_2 for efficient antiviral properties even under dark conditions. Cu_xO nanoclusters were facilely grafted onto TiO_2 powder by a method similar to that used for the fabrication of Cu(II)/TiO_2. Different from the case of Cu(II)/TiO_2 synthesis, we added sodium hydroxide and glucose to the aqueous solution of copper chloride for the grafting process [33]. Glucose dissolved in an alkaline solution acts as a reducing agent of Cu(II) into Cu(I) species; thus, we could control the ratio of Cu(II)/Cu(I) in the Cu_xO nanoclusters by the concentration of glucose and sodium hydroxide in the aqueous solution [33].

Figure 10a shows the TEM image of Cu_xO/TiO_2. Nanoclusters of Cu_xO were well dispersed on the surfaces of TiO_2. In the X-ray diffraction (XRD) pattern of Cu_xO/TiO_2 [33], no additional peaks other than those of TiO_2 were observed, indicating the amorphous nature of the Cu_xO nanoclusters. Figure 10b shows the XANES spectra of Cu_xO/TiO_2 with the reference data of commercial Cu_2O and $Cu(OH)_2$ powders. Peaks I and II are assigned to Cu(I) and Cu(II) species, respectively. The Cu_xO nanoclusters contained both Cu(I) and Cu(II) species. The ratio of Cu(I)/Cu(II) was estimated by their peak intensities in XANES, and the Cu(I)/Cu(II) ratio of the sample was 1.3, which is the optimum ratio to maintain efficient photocatalytic visible-light activity and sustain antiviral properties, which will be discussed later.

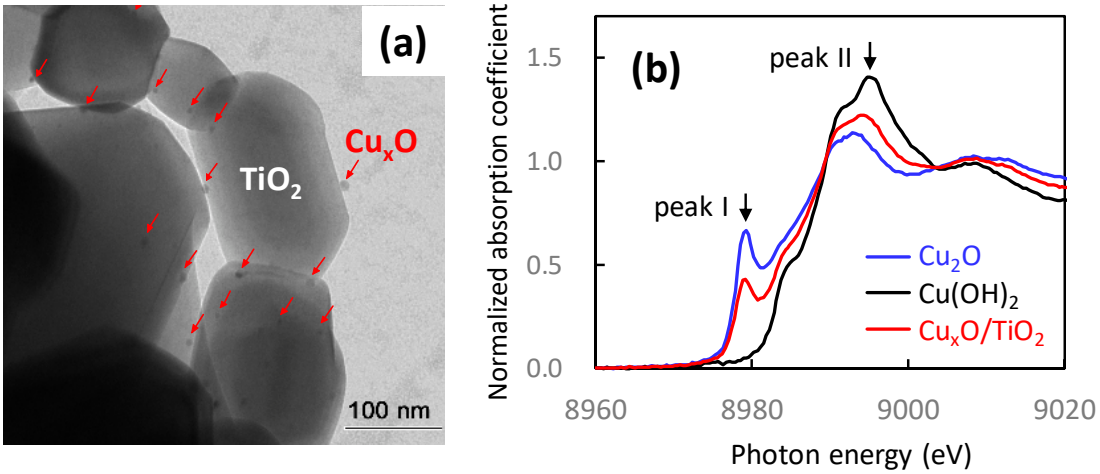

Figure 10. (**a**) TEM image of Cu_xO/TiO_2 and (**b**) XANES spectra of Cu_2O, $Cu(OH)_2$, and Cu_xO/TiO_2 [33].

Figure 11a shows the optical absorption spectrum of Cu_xO/TiO_2. In addition to the intrinsic inter-band absorption below 400 nm of TiO_2, the absorption band assigned to the IFCT in the range of 400–500 nm [26,27], and the absorption over 650 nm attributable to the d-d transition of the Cu(II) species [57], all of which were observed with Cu(II)/TiO_2, as described in the previous section. The Cu_xO/TiO_2 nanocomposites showed an additional absorption band in the range of 500–600 nm, owing to the inter-band transition of Cu_2O [87].

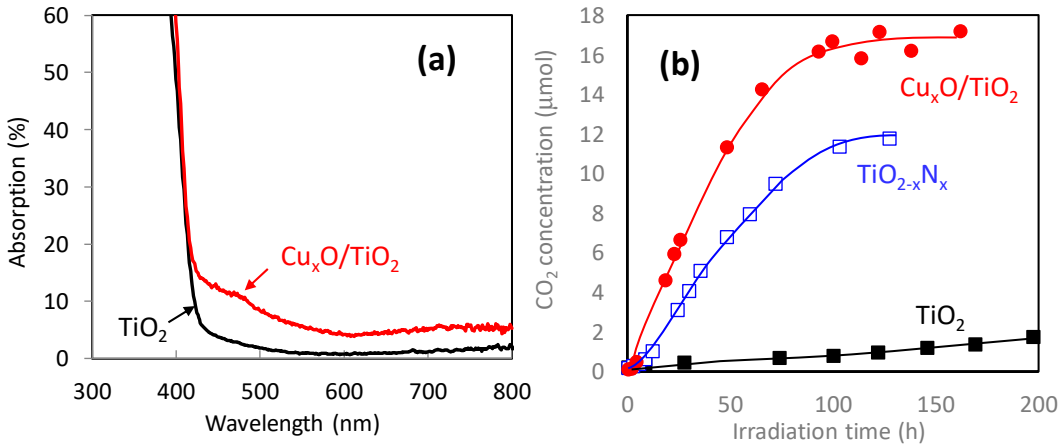

Figure 11. (**a**) Optical absorption spectra of TiO_2 (black line) and Cu_xO/TiO_2 (red line). (**b**) Photocatalytic oxidation activities of 2-propanol under visible-light irradiation for bare TiO_2 (black), $TiO_{2-x}N_x$ (blue), and Cu_xO/TiO_2 (red) [33]. Visible-light irradiation was conducted using a xenon lamp passed through optical filters to set the wavelength at 400–530 nm with an illuminance of 1 mW/cm^2. The ratio of Cu(I)/Cu(II) in Cu_xO was 1.3.

Figure 11b shows the photocatalytic oxidation activities of gaseous 2-propanol to carbon dioxide (CO_2) under visible-light irradiation. In addition to the Cu_xO/TiO_2 composite, we evaluated the photocatalytic activities of TiO_2 and nitrogen-doped TiO_2 ($TiO_{2-x}N_x$) as control groups. The photocatalytic oxidation activity of Cu_xO/TiO_2 was superior to those of TiO_2 and $TiO_{2-x}N_x$ and comparable to the Cu(II)/TiO_2 result [Figure 7b]. It is noted that the photocatalytic oxidation activity depends on the ratio of Cu(I)/Cu(II) [33]. A higher content of Cu(II) is better for photocatalytic oxidation activity. The ratio of Cu(I)/Cu(II) in the study sample was 1.3 [33], which optimized to exhibit high photocatalytic activity as well as antiviral activity under dark conditions, which is discussed below.

Figure 12 shows the antiviral properties of Cu_xO/TiO_2 under white-light irradiation and dark conditions in comparison with $TiO_{2-x}N_x$. The Cu_xO/TiO_2 displayed a 4-log reduction (i.e., a 99.9 9%

reduction of bacteriophage Qβ) after 1 h of contact time under dark conditions, which was significantly superior to the antiviral activity of Cu(II)/TiO_2 under dark conditions (Figure 8, black circles). The antiviral activity of Cu_xO/TiO_2 was further improved under visible-light irradiation as a 7.5-log reduction of bacteriophage was achieved after 40 min. The Cu(I) species in Cu_xO nanoclusters can denature proteins and lose virus activity under dark conditions. Also, the Cu(II) species in the Cu_xO nanocluster accepts electrons from the valence band of TiO_2 to form a Cu(I) species through photo-induced IFCT transition. Therefore, both antiviral active species, i.e., the Cu(I) species and holes in the valence band of TiO_2, are simultaneously created in the Cu_xO/TiO_2 system under visible-light irradiation, exhibiting efficient antiviral function under both visible-light irradiation and dark conditions.

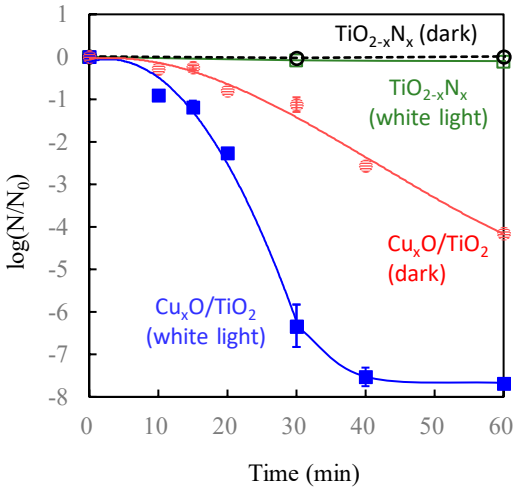

Figure 12. Inactivation of bacteriophage Qβ for various samples. Cu_xO/TiO_2 under white light (blue), Cu_xO/TiO_2 under dark conditions (red), $TiO_{2-x}N_x$ under white light (green), and $TiO_{2-x}N_x$ under dark conditions (black) [33]. Light irradiation was conducted using a commercial 10 W cylindrical white fluorescent lightbulb with a UV cut-off film at an illuminance of 800 lux.

Here, we discuss the optimum ratio of Cu(I)/Cu(II) for both photocatalytic visible light-activity and antiviral properties under dark conditions. We previously evaluated the visible-light activities of Cu_xO/TiO_2 samples with Cu(I)/Cu(II) ratios of 0.13, 0.2, and 1.3 [33], and those activities were comparable to that of Cu(II)/TiO_2. We also investigated the degradation activity of DNA, which is an essential component of viruses, for the various Cu_xO/TiO_2 samples with different Cu(I)/Cu(II) ratios and pristine TiO_2 as a control group [33]. Figure 13 shows the resulting agarose gel electrophoresis patterns after the exposure of supercoiled plasmid pBR322 DNA to various samples for 2 h under dark conditions. Among the examined samples, bare TiO_2 did not cleave the plasmid DNA; however, conversion of the plasmid DNA from the supercoiled to the open circular form was clearly observed in the systems of the hybrid Cu_xO/TiO_2 nanocomposites. Notably, the degradation activity was enhanced as the ratio of Cu(I)/Cu(II) in the hybrid Cu_xO/TiO_2 nanocomposites increased. The complete conversion of supercoiled DNA was achieved using a Cu_xO/TiO_2 [Cu(I)/Cu(II) = 1.3] sample. These results suggest that the hybrid Cu_xO/TiO_2 nanocomposites can destroy the critical biomolecules of viruses, leading to their death and inactivation, even under dark conditions.

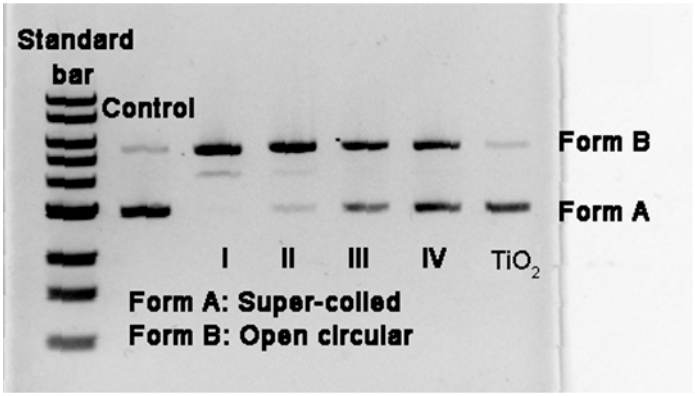

Figure 13. The cleavage of supercoiled plasmid pBR322 DNA by different samples under dark conditions for 2 h [33]. Lanes I, II, III, and IV correspond to Cu(I)/Cu(II) = 1.3, 0.2, 0.13 and Cu(II)/TiO_2, respectively.

Next, we investigated the long-term antiviral properties of Cu_xO/TiO_2 [Cu(I)/Cu(II) = 1.3] according to the following procedure using bacteriophage Qβ. First, the as-prepared Cu_xO/TiO_2 sample was initially examined under dark conditions [label (i) in Figure 14]. Second, the sample stored under ambient air conditions for more than 6 years was examined [label (ii) in Figure 14]. Third, the stored sample was irradiated with white light for 4 days, and its antiviral properties were evaluated under dark conditions [label (iii) in Figure 14]. The initial activity of Cu_xO/TiO_2 decreased under ambient air exposure by self-oxidation [(i)→(ii)], similar to the results for bare Cu_2O shown in Figure 5. However, the deteriorated activity after air exposure was significantly recovered by light irradiation for 4 days. These results imply that the oxidized Cu(II) species in Cu_xO can be recovered to Cu(I) species by light irradiation. Such a recovery function has never been observed in a pristine Cu_2O sample or other solid-state antiviral materials. In contrast to conventional antiviral solid materials, our Cu_xO/TiO_2 maintains its efficient antiviral function, even when light illumination is turned on during the day and off during the night.

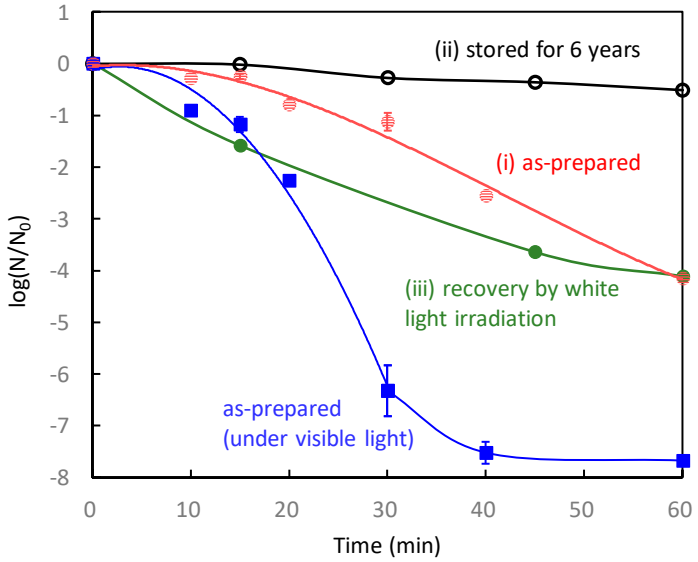

Figure 14. Inactivation of bacteriophage Qβ by Cu_xO/TiO_2 [Cu(I)/Cu(II) = 1.3] under the following sequential conditions: (i) as-prepared sample in the dark (red), (ii) the sample stored under ambient air for more than 6 years (black), (iii) after light irradiation onto the 6-year stored sample for 4 days (green). The antiviral tests of (i)–(iii) were performed under dark conditions. The results of the as-prepared Cu_xO/TiO_2 sample under visible-light irradiation are also shown (blue).

Figure 15 shows a schematic illustration of the working principle of the present antiviral Cu_xO/TiO_2 photocatalyst. Cu(I) species disinfect viruses by denaturalizing their protein under dark conditions. Under light irradiation, photogenerated holes oxidize the organic components of the viruses. Further, light irradiation continuously produces Cu(I) species to suppress the self-oxidation of Cu_xO, resulting in sustained antiviral properties.

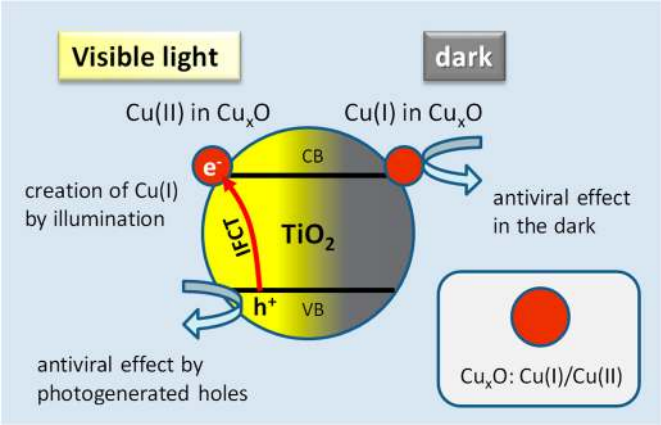

Figure 15. Schematic illustration of the working principle of the antiviral Cu_xO/TiO_2 photocatalyst.

Table 1 summarizes the comparison of the antiviral properties of various copper-based compounds. The antiviral activity of pristine CuO is negligible. Conversely, pristine Cu_2O exhibits efficient antiviral properties at its initial use; however, its initial red colour turns black by self-oxidation to change into Cu(II) inactive species [51,52]. Further, $Cu(II)/TiO_2$ shows photocatalytic oxidation activity under visible light because of the IFCT transition, but its antiviral activity is limited because of the lack of Cu(I) species. Among these samples, the Cu_xO/TiO_2 composite exhibited good antiviral activity under both light irradiation and dark conditions.

Table 1. The comparison of antiviral properties of various copper based compounds.

Material	Antiviral Activity Under Dark Condition	Photocatalytic Activity	Antiviral Activity for Long Term in Indoor Condition
CuO	×	×	×
Cu_2O	○	×	△
$Cu(II)/TiO_2$	×	○	△
Cu_xO/TiO_2	○	○	○

(○: good, △: fair, ×: poor).

5. Viruses Droplet Splash Test of Cu_xO/TiO_2 Photocatalyst

Considering the practical application of the Cu_xO/TiO_2 photocatalyst, we conducted antiviral tests on the Cu_xO/TiO_2-coated sheet fabrics using the pseudo splash-containing bacteriophage Qβ. Figure 16 shows a photograph of the experimental setup for the antiviral splash test. An atomizer generated an aerosol that contained 6×10^7 pfu/h of bacteriophage Qβ, and the particle size of the aerosol was approximately 0.3 μm. The virus aerosol from the atomizer attached to the photocatalyst sheets on a desk of 1 m high from the floor under white fluorescence light at an illuminance of 1000 lux. After 4 h, the number of bacteriophages was counted using the same procedure with the previous studies [33–35]. Bacteriophages on a control sheet without Cu_xO/TiO_2 coating were also sampled at 1 h and 2 h.

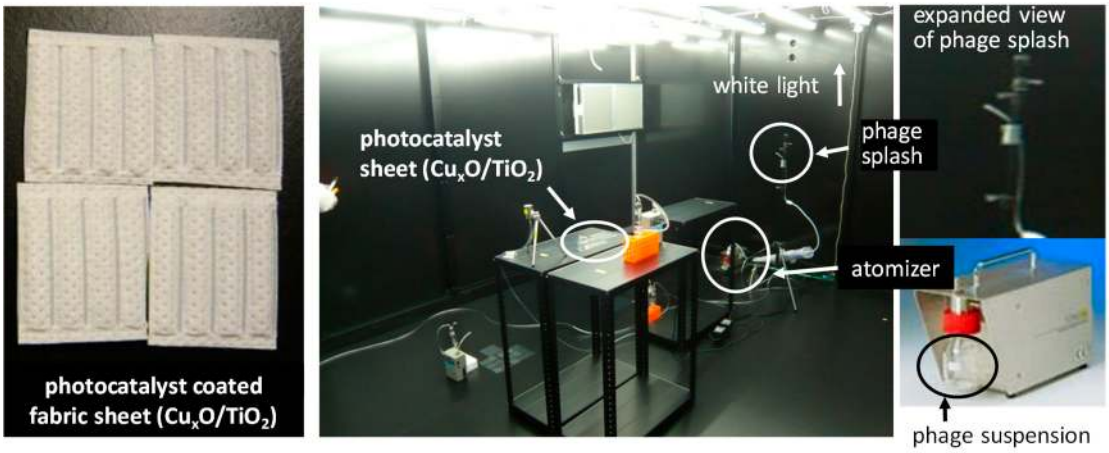

Figure 16. Procedure for evaluating an antiviral Cu_xO/TiO_2-coated fabric sheet using pseudo splash-containing bacteriophage Qβ. Room volume was (4 m × 3 m × 2 m) and the ventilation frequency was 1.8 time/h. White light was irradiated by fluorescent lightbulbs at an illuminance of 1000 lux. Bacteriophage Qβ containing 6×10^7 pfu/h was sprayed for 4 h by an atomizer (ATM-226, KANOMAX JAPAN INC.) to attach it on the sheet surfaces.

Figure 17 shows the changes in the number of bacteriophages on the photocatalyst sheet and control sheet. It is noteworthy that the number of bacteriophages on the Cu_xO/TiO_2 sheet was negligible, indicating its strong antiviral function against the virus attached to the surface. A Cu_xO/TiO_2-coated material can thus potentially disinfect viruses on any surface derived from droplets and aerosol to protect against viral disease spread by contact infection.

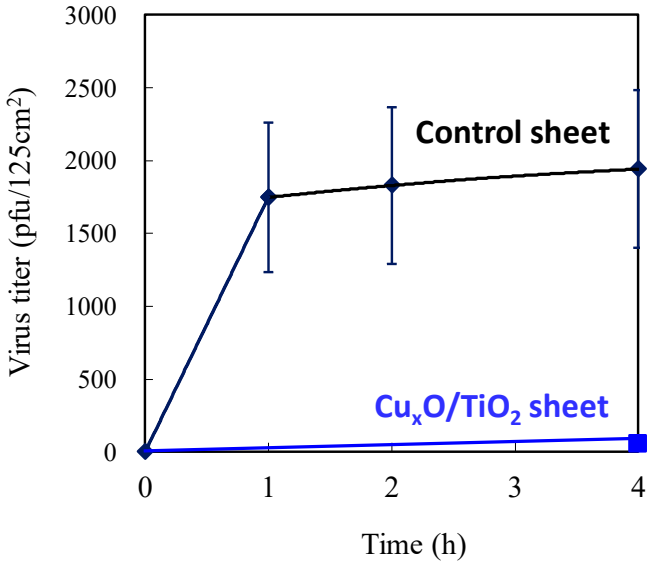

Figure 17. Antiviral properties of the Cu_xO/TiO_2-coated sheet and the control sheet without the photocatalyst using splash-containing bacteriophage Qβ. In the case of Cu_xO/TiO_2 to avoid the overestimation of its antiviral property, the number of experiments was set to 1 time (after 4h) in order to exclude the influence of air flow due to human's entering into the room for measurement.

6. Conclusions

This review paper introduces the recent progress in the development of Cu_xO/TiO_2 as an efficient visible light-sensitive photocatalyst for antiviral applications. The Cu_xO nanocluster consists of the valence states of Cu(I) and Cu(II). Cu(I) species in Cu_xO nanoclusters can denature viral proteins, resulting in significant antiviral properties even under dark conditions. Unfortunately, the Cu(I) species

in Cu_xO are easily oxidized to inactive Cu(II) in ambient air. However, the combination of Cu_xO with the TiO_2 photocatalyst maintained its antiviral function by visible-light irradiation. In the Cu_xO/TiO_2 photocatalyst, electron transition occurs by visible-light irradiation through the IFCT process; this results in the generation of antiviral Cu(I) species and holes in the valence band of TiO_2, which are effective in disinfecting viruses. Once the Cu(I) species in Cu_xO turn into Cu(II) by self-oxidation, antiviral active Cu(I) species can be regenerated by visible light like a white fluorescence bulb. Therefore, the antiviral function of Cu_xO/TiO_2 can be maintained, even under indoor conditions, where light illumination is turned on during the day and off during the night. It is also noted that the Cu_xO/TiO_2 composite samples have been commercialized (NAKA CORPORATION, Tokyo Japan). We expect the Cu_xO/TiO_2 material to be applied to various antiviral industrial items in indoor circumstances, such as hospitals, airports, metro stations, and schools, as coating materials for air filters, respiratory face masks, and antifungal fabrics to prevent the COVID-19 spread. Furthermore, the present concept contributes to the design of various antiviral materials, such as bimetallic catalysts [88–90].

Author Contributions: Conceptualization, K.H.; antiviral investigation, K.S.; photocatalysis investigation, M.M.; writing—original draft preparation, M.M.; writing—review and editing, K.H.; project leader, K.H. All authors have read and agreed to the published version of the manuscript.

Funding: This research was funded by New Energy and Industrial Technology Development Organisation (NEDO) in Japan, project name: Project to Create Photocatalyst Industry for Recycling-Oriented Society. This research was also funded by JSPS Kakenhi, grant No. 18H02055.

Acknowledgments: We appreciate the project members of NEDO, including H. Irie at Yamanashi University, Japan, M. Minoshima at Osaka University, Japan, Y. Kuroda at Showa Denko K.K., Japan, H. Yu at Wuhan University of Technology, China, X. Qiu and M. Liu at Central South University, China, and other collaborators for their great help in the development of the present photocatalyst. Nitrogen-doped TiO_2 ($TiO_{2-x}N_x$) was provided by Showa Denko K.K. (HP-N08).

Conflicts of Interest: The authors declare no conflict of interest.

References

1. Morens, D.M.; Folkers, G.K.; Fauci, A.S. The challenge of emerging and re-emerging infectious diseases. *Nature* **2004**, *430*, 242–249. [CrossRef] [PubMed]
2. Leroy, E.M.; Kumulungui, B.; Pourrut, X.; Rouquet, P.; Hassanin, A.; Yaba, P.; Délicat, A.; Paweska, J.T.; Gonzalez, J.P.J.; Swanepoel, R. Fruit bats as reservoirs of Ebola virus. *Nature* **2005**, *438*, 575–576. [CrossRef] [PubMed]
3. Vijaykrishna, D.; Poon, L.L.M.; Zhu, H.C.; Ma, S.K.; Li, O.T.W.; Cheung, C.L.; Smith, G.J.D.; Peiris, J.S.M.; Guan, Y. Reassortment of pandemic h1n1/2009 influenza a virus in swine. *Science* **2010**, *328*, 1529. [CrossRef] [PubMed]
4. Wölfel, R.; Corman, V.M.; Guggemos, W.; Seilmaier, M.; Zange, S.; Müller, M.A.; Niemeyer, D.; Jones, T.C.; Vollmar, P.; Rothe, C.; et al. Virological assessment of hospitalized patients with COVID-2019. *Nature* **2020**, *581*, 465–469. [CrossRef] [PubMed]
5. Brankston, G.; Gitterman, L.; Hirji, Z.; Lemieux, C.; Gardam, M. Transmission of influenza A in human beings. *Lancet Infect. Dis.* **2007**, *7*, 257–265. [CrossRef]
6. Kampf, G.; Grotheer, D.; Steinmann, J. Efficacy of three ethanol-based hand rubs against feline calicivirus, a surrogate virus for norovirus. *J. Hosp. Infect.* **2005**, *60*, 144–149. [CrossRef]
7. Tuladhar, E.; Terpstra, P.; Koopmans, M.; Duizer, E. Virucidal efficacy of hydrogen peroxide vapour disinfection. *J. Hosp. Infect.* **2012**, *80*, 110–115. [CrossRef]
8. Barclay, L.; Park, G.W.; Vega, E.; Hall, A.; Parashar, U.; Vinjé, J.; Lopman, B. Infection control for norovirus. *Clin. Microbiol. Infect.* **2014**, *20*, 731–740. [CrossRef]
9. Anson, M. Protein denaturation and the properties of protein groups. In *Advances in Protein Chemistry*; Anson, M.L., Edsall, J.T., Eds.; Academic Press: Cambridge, MA, USA, 1945; Volume 2, pp. 361–386.
10. Thurman, R.B.; Gerba, C.P.; Bitton, G. The molecular mechanisms of copper and silver ion disinfection of bacteria and viruses. *Crit. Rev. Environ. Control.* **1989**, *18*, 295–315. [CrossRef]
11. Sunada, K.; Kikuchi, Y.; Hashimoto, K.; Fujishima, A. Bactericidal and detoxification effects of TiO_2 thin film Photocatalysts. *Environ. Sci. Technol.* **1998**, *32*, 726–728. [CrossRef]

12. Sunada, K.; Watanabe, T.; Hashimoto, K. Studies on photokilling of bacteria on TiO2 thin film. *J. Photochem. Photobiol. A Chem.* **2003**, *156*, 227–233. [CrossRef]
13. Sunada, K.; Watanabe, T.; Hashimoto, K. Bactericidal activity of copper-deposited TiO_2 thin film under weak UV light illumination. *Environ. Sci. Technol.* **2003**, *37*, 4785–4789. [CrossRef]
14. Hajkova, P.; Spatenka, P.; Horsky, J.; Horska, I.; Kolouch, A. Photocatalytic effect of TiO_2 films on viruses and bacteria. *Plasma Process. Polym.* **2007**, *4*, S397–S401. [CrossRef]
15. Ishiguro, H.; Nakano, R.; Yao, Y.; Kajioka, J.; Fujishima, A.; Sunada, K.; Minoshima, A.M.; Hashimoto, K.; Kubota, Y. Photocatalytic inactivation of bacteriophages by TiO_2-coated glass plates under low-intensity, long-wavelength UV irradiation. *Photochem. Photobiol. Sci.* **2011**, *10*, 1825–1829. [CrossRef]
16. Nakano, R.; Ishiguro, H.; Yao, Y.; Kajioka, J.; Fujishima, A.; Sunada, K.; Minoshima, A.M.; Hashimoto, K.; Kubota, Y. Photocatalytic inactivation of influenza virus by titanium dioxide thin film. *Photochem. Photobiol. Sci.* **2012**, *11*, 1293–1298. [CrossRef] [PubMed]
17. Fujishima, A.; Rao, T.N.; Tryk, D.A. Titanium dioxide photocatalysis. *J. Photochem. Photobiol. C Photochem. Rev.* **2000**, *1*, 1–21. [CrossRef]
18. Mills, A.; Le Hunte, S. An overview of semiconductor photocatalysis. *J. Photochem. Photobiol. A Chem.* **1997**, *108*, 1–35. [CrossRef]
19. Hoffmann, M.R.; Martin, S.T.; Choi, W.; Bahnemann, D.W. Environmental applications of semiconductor photocatalysis. *Chem. Rev.* **1995**, *95*, 69–96. [CrossRef]
20. Paz, Y.; Luo, Z.; Rabenberg, L.; Heller, A. Photooxidative self-cleaning transparent titanium dioxide films on glass. *J. Mater. Res.* **1995**, *10*, 2842–2848. [CrossRef]
21. Wang, R.; Hashimoto, K.; Fujishima, A.; Chikuni, M.; Kojima, E.; Kitamura, A.; Shimohigoshi, M.; Watanabe, T. Light-induced amphiphilic surfaces. *Nature* **1997**, *388*, 431–432. [CrossRef]
22. Wang, R.; Hashimoto, K.; Fujishima, A.; Chikuni, M.; Kojima, E.; Kitamura, A.; Shimohigoshi, M.; Watanabe, T. Photogeneration of highly amphiphilic tio_2 surfaces. *Adv. Mater.* **1998**, *10*, 135–138. [CrossRef]
23. Miyauchi, M.; Nakajima, A.; Hashimoto, K.; Watanabe, T. A highly hydrophilic thin film under 1 μW/cm2 UV illumination. *Adv. Mater.* **2000**, *12*, 1923–1927. [CrossRef]
24. Miyauchi, M.; Nakajima, A.; Watanabe, T.; Hashimoto, K. Photocatalysis and photoinduced hydrophilicity of various metal oxide thin films. *Chem. Mater.* **2002**, *14*, 2812–2816. [CrossRef]
25. Miyauchi, M.; Tokudome, H. Highly hydrophilic conversion on oriented TiO_2 thin films synthesized by a facile spin-coating method. *Appl. Phys. Lett.* **2007**, *91*, 43111. [CrossRef]
26. Irie, H.; Miura, S.; Kamiya, K.; Hashimoto, K. Efficient visible light-sensitive photocatalysts: Grafting Cu(II) ions onto TiO_2 and WO_3 photocatalysts. *Chem. Phys. Lett.* **2008**, *457*, 202–205. [CrossRef]
27. Irie, H.; Kamiya, K.; Shibanuma, T.; Miura, S.; Tryk, D.A.; Yokoyama, T.; Hashimoto, K. Visible light-sensitive cu(II)-grafted TiO_2 photocatalysts: Activities and X-ray absorption fine structure analyses. *J. Phys. Chem. C* **2009**, *113*, 10761–10766. [CrossRef]
28. Liu, M.; Qiu, X.; Miyauchi, M.; Hashimoto, K. Cu(II) oxide amorphous nanoclusters grafted Ti_3+self-doped TiO_2: An efficient visible light photocatalyst. *Chem. Mater.* **2011**, *23*, 5282–5286. [CrossRef]
29. Liu, M.; Inde, R.; Nishikawa, M.; Qiu, X.; Atarashi, D.; Sakai, E.; Nosaka, Y.; Hashimoto, K.; Miyauchi, M. Enhanced photoactivity with nanocluster-grafted titanium dioxide photocatalysts. *ACS Nano* **2014**, *8*, 7229–7238. [CrossRef]
30. Miyauchi, M.; Liu, Z.; Zhao, Z.-G.; Anandan, S.; Tokudome, H. Visible-light-driven superhydrophilicity by interfacial charge transfer between metal ions and metal oxide nanostructures. *Langmuir* **2010**, *26*, 796–801. [CrossRef]
31. Miyauchi, M.; Irie, H.; Liu, M.; Qiu, X.; Yu, H.; Sunada, K.; Hashimoto, K. Visible-light-sensitive photocatalysts: Nanocluster-grafted titanium dioxide for indoor environmental remediation. *J. Phys. Chem. Lett.* **2016**, *7*, 75–84. [CrossRef]
32. Liu, M.; Sunada, K.; Hashimoto, K.; Miyauchi, M. Visible-light sensitive Cu(II)–TiO_2 with sustained anti-viral activity for efficient indoor environmental remediation. *J. Mater. Chem. A* **2015**, *3*, 17312–17319. [CrossRef]
33. Qiu, X.; Miyauchi, M.; Sunada, K.; Minoshima, A.M.; Liu, M.; Lu, Y.; Li, D.; Shimodaira, Y.; Hosogi, Y.; Kuroda, Y.; et al. Hybrid CuxO/TiO_2 nanocomposites as risk-reduction materials in indoor environments. *ACS Nano* **2012**, *6*, 1609–1618. [CrossRef] [PubMed]
34. Sunada, K.; Minoshima, A.M.; Hashimoto, K. Highly efficient antiviral and antibacterial activities of solid-state cuprous compounds. *J. Hazard. Mater.* **2012**, *235–236*, 265–270. [CrossRef]

35. Minoshima, A.M.; Lü, Y.; Kimura, T.; Nakano, R.; Ishiguro, H.; Kubota, Y.; Hashimoto, K.; Sunada, K. Comparison of the antiviral effect of solid-state copper and silver compounds. *J. Hazard. Mater.* **2016**, *312*, 1–7. [CrossRef]
36. Deka, P.; Borah, B.J.; Saikia, H.; Bharali, P. Cu-based nanoparticles as emerging environmental catalysts. *Chem. Rec.* **2019**, *19*, 462–473. [CrossRef]
37. Scotti, N.; Monticelli, D.; Zaccheria, F. Dispersed copper oxide: A multifaceted tool in catalysis. *Inorganica Chim. Acta* **2012**, *380*, 194–200. [CrossRef]
38. Ren, G.; Hu, D.; Cheng, E.W.; Vargas-Reus, M.A.; Reip, P.; Allaker, R.P. Characterisation of copper oxide nanoparticles for antimicrobial applications. *Int. J. Antimicrob. Agents* **2009**, *33*, 587–590. [CrossRef]
39. Pang, H.; Gao, F.; Lu, Q. Morphology effect on antibacterial activity of cuprous oxide. *Chem. Commun.* **2009**, *9*, 1076–1078. [CrossRef]
40. Borkow, G.; Zhou, S.S.; Page, T.; Gabbay, J. A Novel anti-influenza copper oxide containing respiratory face mask. *PLoS ONE* **2010**, *5*, e11295. [CrossRef]
41. Imlay, J.A. Pathways of oxidative damage. *Annu. Rev. Microbiol.* **2003**, *57*, 395–418. [CrossRef]
42. Nilsson, J.O.; Tornkvist, C.; Liedberg, B. Photoelectron and infrared reflection absorption spectroscopy of benzotriazole adsorbed on copper and cuprous oxide surfaces. *Appl. Surf. Sci.* **1989**, *37*, 306–326. [CrossRef]
43. Chernousova, S.; Epple, M. ChemInform abstract: Silver as antibacterial agent: Ion, nanoparticle, and metal. *Angew. Chem. Int.* **2013**, *52*, 1636–1653. [CrossRef] [PubMed]
44. Glover, R.D.; Miller, J.M.; Hutchison, J.E. Generation of metal nanoparticles from silver and copper objects: Nanoparticle dynamics on surfaces and potential sources of nanoparticles in the environment. *ACS Nano* **2011**, *5*, 8950–8957. [CrossRef] [PubMed]
45. Alexander, J.W. History of the medical use of silver. *Surg. Infect.* **2009**, *10*, 289–292. [CrossRef] [PubMed]
46. Panáček, A.; Kvítek, L.; Prucek, R.; Kolář, M.; Večeřová, R.; Pizúrová, N.; Sharma, V.K.; Nevěčná, T.; Zbořil, R. Silver colloid nanoparticles: Synthesis, characterization, and their antibacterial activity. *J. Phys. Chem. B* **2006**, *110*, 16248–16253. [CrossRef] [PubMed]
47. Das, K.; Aramini, J.M.; Ma, L.C.; Krug, R.M.; Arnold, E. Structures of influenza A proteins and insights into antiviral drug targets. *Nat. Struct. Mol. Biol.* **2010**, *17*, 530–538. [CrossRef]
48. Matrosovich, M.N.; Matrosovich, T.Y.; Gray, T.; Roberts, N.A.; Klenk, H.D. Neuraminidase is important for the initiation of influenza virus infection in human airway epithelium. *J. Virol.* **2004**, *78*, 12665–12667. [CrossRef]
49. Donald, H.B.; Isaacs, A. Counts of influenza virus particles. *J. Gen. Microbiol.* **1954**, *10*, 457–464. [CrossRef]
50. Buxton, R.C.; Edwards, B.; Juo, R.R.; Voyta, J.C.; Tisdale, M.; Bethell, R.C. Development of a sensitive chemiluminescent neuraminidase assay for the determination of influenza virus susceptibility to zanamivir. *Anal. Biochem.* **2000**, *280*, 291–300. [CrossRef]
51. Gattinoni, C.; Michaelides, A. Atomistic details of oxide surfaces and surface oxidation: The example of copper and its oxides. *Surf. Sci. Rep.* **2015**, *70*, 424–447. [CrossRef]
52. Platzman, I.; Brener, R.; Haick, H.; Tannenbaum, R. Oxidation of polycrystalline copper thin films at ambient conditions. *J. Phys. Chem. C* **2008**, *112*, 1101–1108. [CrossRef]
53. Nian, J.N.; Chen, S.A.; Tsai, C.C.; Teng, H. Structural feature and catalytic performance of cu species distributed over TiO_2 nanotubes. *J. Phys. Chem. B* **2006**, *110*, 25817–25824. [CrossRef] [PubMed]
54. Hsiung, T.L.; Wang, H.P.; Lu, Y.M.; Hsiao, M.C. In situ XANES studies of CuO/TiO_2 thin films during photocatalytic degradation of $CHCl_3$. *Radiat. Phys. Chem.* **2006**, *75*, 2054–2057. [CrossRef]
55. Okamoto, Y.; Kubota, T.; Gotoh, H.; Ohto, Y.; Aritani, H.; Tanaka, T.; Yoshida, S. XAFS study of zirconia-supported copper catalysts for the NO–CO reaction: Deactivation, rejuvenation and stabilization of Cu species. *J. Chem. Soc. Faraday Trans.* **1998**, *94*, 3743–3752. [CrossRef]
56. Stern, E.A.; Newville, M.; Ravel, B.; Yacoby, Y.; Haskel, D. The UWXAFS analysis package: Philosophy and details. *Phys. B Condens. Matter* **1995**, *208*, 117–120. [CrossRef]
57. Choudhury, B.; Dey, M.; Choudhury, A. Defect generation, d-d transition, and band gap reduction in Cu-doped TiO_2 nanoparticles. *Int. Nano Lett.* **2013**, *3*, 25. [CrossRef]
58. Hush, N. Homogeneous and heterogeneous optical and thermal electron transfer. *Electrochim. Acta* **1968**, *13*, 1005–1023. [CrossRef]
59. Creutz, C.; Brunschwig, B.S.; Sutin, N. Interfacial charge-transfer absorption: Semiclassical treatment. *J. Phys. Chem. B* **2005**, *109*, 10251–10260. [CrossRef]

60. Creutz, C.; Brunschwig, B.S.; Sutin, N. Interfacial charge-transfer absorption: 3. Application to semiconductor−molecule assemblies. *J. Phys. Chem. B* **2006**, *110*, 25181–25190. [CrossRef]
61. Nakamura, R.; Okamoto, A.; Osawa, H.; Irie, H.; Hashimoto, K. Design of all-inorganic molecular-based photocatalysts sensitive to visible light: Ti(iv)−o−ce(iii) bimetallic assemblies on mesoporous silica. *J. Am. Chem. Soc.* **2007**, *129*, 9596–9597. [CrossRef]
62. Yu, H.; Irie, H.; Shimodaira, Y.; Hosogi, Y.; Kuroda, Y.; Miyauchi, M.; Hashimoto, K. An efficient visible-light-sensitive fe(iii)-grafted tio$_2$ photocatalyst. *J. Phys. Chem. C* **2010**, *114*, 16481–16487. [CrossRef]
63. Asahi, R.; Morikawa, T.; Ohwaki, T.; Aoki, K.; Taga, Y. Visible-light photocatalysis in nitrogen-doped titanium oxides. *Science* **2001**, *293*, 269–271. [CrossRef] [PubMed]
64. Sakthivel, S.; Kisch, H. Photocatalytic and photoelectrochemical properties of nitrogen-doped titanium dioxide. *ChemPhysChem* **2003**, *4*, 487–490. [CrossRef] [PubMed]
65. Irie, H.; Watanabe, Y.; Hashimoto, K. Nitrogen-concentration dependence on photocatalytic activity of tio$_2$-xnx powders. *J. Phys. Chem. B* **2003**, *107*, 5483–5486. [CrossRef]
66. Miyauchi, M.; Ikezawa, A.; Tobimatsu, H.; Irie, H.; Hashimoto, K. Zeta potential and photocatalytic activity of nitrogen doped TiO_2 thin films. *Phys. Chem. Chem. Phys.* **2004**, *6*, 865–870. [CrossRef]
67. Nakamura, R.; Tanaka, T.; Nakato, Y. Mechanism for visible light responses in anodic photocurrents at N-doped TiO_2 film electrodes. *J. Phys. Chem. B* **2004**, *108*, 10617–10620. [CrossRef]
68. Nosaka, Y.; Takahashi, S.; Sakamoto, H.; Nosaka, A.Y. Reaction mechanism of cu(ii)-grafted visible-light responsive TiO_2 and WO_3 photocatalysts studied by means of ESR spectroscopy and chemiluminescence photometry. *J. Phys. Chem. C* **2011**, *115*, 21283–21290. [CrossRef]
69. Jung, M.; Hart, J.N.; Scott, J.A.; Ng, Y.H.; Jiang, Y.; Amal, R. Exploring Cu oxidation state on TiO_2 and its transformation during photocatalytic hydrogen evolution. *Appl. Catal. A Gen.* **2016**, *521*, 190–201. [CrossRef]
70. Yeager, E. Electrocatalysts for O_2 reduction. *Electrochim. Acta* **1984**, *29*, 1527–1537. [CrossRef]
71. Wang, Y.; Balbuena, P.B. Ab initio molecular dynamics simulations of the oxygen reduction reaction on a pt(111) surface in the presence of hydrated hydronium (H_3O)+(H_2O)2: Direct or series pathway? *J. Phys. Chem. B* **2005**, *109*, 14896–14907. [CrossRef]
72. Mustain, W.E.; Prakash, J. A model for the electroreduction of molecular oxygen. *J. Electrochem. Soc.* **2007**, *154*, A668–A676. [CrossRef]
73. Osako, K.; Matsuzaki, K.; Hosono, H.; Yin, G.; Atarashi, D.; Sakai, E.; Susaki, T.; Miyauchi, M. Examination of interfacial charge transfer in photocatalysis using patterned CuO thin film deposited on TiO_2. *APL Mater.* **2015**, *3*, 104409. [CrossRef]
74. Osako, K.; Matsuzaki, K.; Susaki, T.; Ueda, S.; Yin, G.; Yamaguchi, A.; Hosono, H.; Miyauchi, M. Direct Observation of interfacial charge transfer between rutile tio$_2$ and ultrathin cuox film by visible-light illumination and its application for efficient photocatalysis. *ChemCatChem* **2018**, *10*, 3666–3670. [CrossRef]
75. Anandan, S.; Ohashi, N.; Miyauchi, M. Zno-based visible-light photocatalyst: Band-gap engineering and multi-electron reduction by co-catalyst. *Appl. Catal. B* **2010**, *100*, 502–509. [CrossRef]
76. Anandan, S.; Miyauchi, M. Ce-doped ZnO ($Ce_xZn_{1-x}O$) becomes an efficient visible-light-sensitive photocatalyst by co-catalyst (Cu^{2+}) grafting. *Phys. Chem. Chem. Phys.* **2011**, *13*, 14937–14945. [CrossRef] [PubMed]
77. Qiu, X.; Miyauchi, M.; Yu, H.; Irie, H.; Hashimoto, K. Visible-light-driven cu(ii)−(sr1−ynay)(ti1−xmox)o3 photocatalysts based on conduction band control and surface ion modification. *J. Am. Chem. Soc.* **2010**, *132*, 15259–15267. [CrossRef]
78. Nosaka, Y.; Takahashi, S.; Mitani, Y.; Qiu, X.; Miyauchi, M. Reaction mechanism of visible-light responsive Cu(II)-grafted Mo-doped $SrTiO_3$ photocatalyst studied by means of ESR spectroscopy and chemiluminescence photometry. *Appl. Catal. B Environ.* **2012**, *111–112*, 636–640. [CrossRef]
79. Pan, S.; Wang, S.; Zhang, Y.; Xu, S.; Kong, F.; Luo, Y.; Tian, Y.; Teng, X.; Li, G. Surface Fe_3+-decorated pristine SnO_2 nanoparticles with enhanced ·OH radical generation performance. *Catal. Commun.* **2012**, *24*, 96–99. [CrossRef]
80. Yin, G.; Nishikawa, M.; Nosaka, Y.; Srinivasan, N.; Atarashi, D.; Sakai, E.; Miyauchi, M. Photocatalytic carbon dioxide reduction by copper oxide nanocluster-grafted niobate nanosheets. *ACS Nano* **2015**, *9*, 2111–2119. [CrossRef]
81. Hu, J.; Li, H.; Huang, C.; Liu, M.; Qiu, X. Enhanced photocatalytic activity of Bi_2O_3 under visible light irradiation by Cu(II) clusters modification. *Appl. Catal. B Environ.* **2013**, *142–143*, 598–603. [CrossRef]

82. Huang, C.; Hu, J.; Cong, S.; Zhao, Z.; Qiu, X. Hierarchical BiOCl microflowers with improved visible-light-driven photocatalytic activity by Fe(III) modification. *Appl. Catal. B Environ.* **2015**, *174*, 105–112. [CrossRef]
83. Yang, Y.; Yamaguchi, A.; Jiang, H.; Van Der Kooy, A.; Okunaka, S.; Hosogai, M.; Tokudome, H.; Miyauchi, M. Green light active photocatalyst for complete oxidation of organic molecules. *Chem. Commun.* **2020**, *56*, 9210–9213. [CrossRef] [PubMed]
84. Wang, P.; Xia, Y.; Wu, P.; Wang, X.; Yu, H.; Yu, J. Cu(II) as a general cocatalyst for improved visible-light photocatalytic performance of photosensitive ag-based compounds. *J. Phys. Chem. C* **2014**, *118*, 8891–8898. [CrossRef]
85. Liu, M.; Qiu, X.; Hashimoto, K.; Miyauchi, M. Cu(ii) nanocluster-grafted, Nb-doped TiO_2 as an efficient visible-light-sensitive photocatalyst based on energy-level matching between surface and bulk states. *J. Mater. Chem. A* **2014**, *2*, 13571–13579. [CrossRef]
86. Yu, H.; Irie, H.; Hashimoto, K. Conduction band energy level control of titanium dioxide: Toward an efficient visible-light-sensitive photocatalyst. *J. Am. Chem. Soc.* **2010**, *132*, 6898–6899. [CrossRef]
87. Banerjee, S.; Chakravorty, D. Optical absorption by nanoparticles of Cu_2O. *EPL Europhys. Lett.* **2000**, *52*, 468–473. [CrossRef]
88. Han, Y.; Wang, Y.; Ma, T.; Li, W.; Zhang, J.; Zhang, M. Mechanistic understanding of Cu-based bimetallic catalysts. *Front. Chem. Sci. Eng.* **2020**, *14*, 689–748. [CrossRef]
89. Spanu, D.; Recchia, S.; Mohajernia, S.; Tomanec, O.; Kment, S.; Zbořil, R.; Schmuki, P.; Altomare, M. Templated dewetting–Alloying of NiCu bilayers on TiO_2 nanotubes enables efficient noble-metal-free photocatalytic H_2 evolution. *ACS Catal.* **2018**, *8*, 5298–5305. [CrossRef]
90. Wysocka, I.; Kowalska, E.; Ryl, J.; Nowaczyk, G.; Zielińska-Jurek, A. Morphology, photocatalytic and antimicrobial properties of TiO_2 modified with mono- and bimetallic copper, platinum and silver nanoparticles. *Nanomaterials* **2019**, *9*, 1129. [CrossRef]